

# Measurement of total phase fluctuation in cold-atomic quantum simulators

Taufiq Murtadho,<sup>1,\*</sup> Federica Cataldini,<sup>2</sup> Sebastian Erne,<sup>2</sup> Marek Gluza,<sup>1</sup> Jörg Schmiedmayer,<sup>2</sup> and Nelly H.Y. Ng<sup>1,†</sup>

<sup>1</sup>*School of Physical and Mathematical Sciences, Nanyang Technological University, 639673 Singapore*

<sup>2</sup>*Vienna Center for Quantum Science and Technology, Atominstitut, TU Wien, Stadionallee 2, 1020 Vienna, Austria*

(Dated: August 8, 2024)

Studying the dynamics of quantum many-body systems is often constrained by the limitations in probing relevant observables, especially in continuous systems. A prominent example is two parallel 1D Bose gases, which simulate 1D quantum field theories through the phase difference probed by interference. Here we introduce a method to extract the total phase of the combined system based on a general principle of reconstructing phase gradient from density dynamics using continuity equation. This approach reveals the previously hidden sector of the sum mode of the two 1D Bose gases. We validate our technique numerically and demonstrate its effectiveness by analysing data from selected experiments, showcasing how our method expands the scope and capabilities of cold-atomic quantum simulators.

*Introduction.*— Quantum many-body systems are quantum simulators for a large variety of systems in and out of equilibrium [1–3]. In particular, ultracold atoms have emerged as a powerful and versatile platform for simulating discrete [4–6] and continuous variable (i.e. quantum field) [7] systems. A notably powerful example of the latter are one dimensional (1D) superfluids, which have enabled the observation of pre-thermalization [8] light cone dynamics [9, 10], generalized statistical ensembles [11], recurrences [12], the area law of mutual information [13], Landauer erasure [14], and the strongly correlated Sine-Gordon field theory through the evaluation of many-body correlations [15, 16].

All of these studies are based on extracting the local *relative* phase of two parallel 1D superfluids by measuring interference after free expansion [17–19]. In the case of Gaussian states, its canonical conjugate—the relative density fluctuation—can also be reconstructed from relative phase data utilizing a coherent Tomonaga-Luttinger liquid evolution [20]. However, the relative phase and relative density fluctuations are still only two out of the four fields characterizing the system. The remaining two fields belong to the total sector, i.e. the sum rather than the difference of fluctuations in both density and phases, have insofar been inaccessible in experiments. Knowledge about the dynamics in the total sector becomes important when studying long-time thermalisation behaviour [21–23] or testing the validity of the quantum field simulators [8–16], which rely on a separation of the difference and total sector.

Here we present a method to obtain single-shot information for the total phase and its fluctuations in two parallel quasi-condensates from the measured density ripple (matter wave speckles) [24–28] after free expansion. The physical principle behind our extraction is the continuity equation which connects the density ripple patterns to the full counting statistics of the phase gradients associated with the current operator. We validate our extraction numerically and experimentally by reconstructing

total phase signals from thermal states and for a strongly excited mode in driven Luttinger liquids.

*Extracting total phase for a pair of superfluids from density ripples.*— We first consider two parallel and separated quasicondensates each described by bosonic phase  $\hat{\phi}_a(\mathbf{r})$  and density fields  $\hat{n}_a(\mathbf{r})$  where  $a = 1, 2$ . We show how to extract the statistics of the total phase

$$\hat{\phi}_+(\mathbf{r}) = \hat{\phi}_1(\mathbf{r}) + \hat{\phi}_2(\mathbf{r}) \quad (1)$$

at  $t = 0$  from single-shot measurements of total density  $\hat{n}_+(\mathbf{r}, t) = \hat{n}_1(\mathbf{r}, t) + \hat{n}_2(\mathbf{r}, t)$  following a unitary evolution  $t > 0$  (e.g. time of flight). Our method is motivated by experiments which give access to  $\hat{n}_+(\mathbf{r}, t)$ .

Each gas satisfies a continuity equation  $\partial_t \hat{n}_a(\mathbf{r}, t) + \nabla \cdot \hat{\mathbf{j}}_a(\mathbf{r}, t) = 0$  with  $\hat{\mathbf{j}}_a(\mathbf{r}, t) = (\hbar/m)n_a(\mathbf{r}, t)\nabla\hat{\phi}_a(\mathbf{r}, t)$  is the current operator and  $n_a(\mathbf{r}, t) = \langle \hat{n}_a(\mathbf{r}, t) \rangle$  is the mean density. We consider short time-scales where the continuity equation for  $\hat{n}_+(\mathbf{r}, t)$  can be linearized as

$$\hat{n}_+(\mathbf{r}, t) \approx \hat{n}_+(\mathbf{r}, 0) - t\nabla \cdot \hat{\mathbf{j}}_+(\mathbf{r}, 0), \quad (2)$$

with  $\hat{\mathbf{j}}_+ = \hat{\mathbf{j}}_1 + \hat{\mathbf{j}}_2$  being the total current. For the special case of equal mean density  $n_1(\mathbf{r}) = n_2(\mathbf{r}) = n_0(\mathbf{r})/2$ , the total current is proportional to the gradient of total phase  $\nabla\hat{\phi}_+(\mathbf{r})$ , i.e. the observable we want to measure. Meanwhile, the initial condition is  $\hat{n}_+(\mathbf{r}, 0) = n_0(\mathbf{r}) + \delta\hat{n}_+(\mathbf{r})$  where  $\delta\hat{n}_+(\mathbf{r}) = \delta\hat{n}_1(\mathbf{r}) + \delta\hat{n}_2(\mathbf{r})$  is the total initial density fluctuation, which we will ignore for the extraction.

If we further assume smooth enough trapping potential so that the mean density  $n_0(\mathbf{r})$  varies little on the length scale of the measurement dynamics  $\ell_t \equiv \sqrt{\hbar t/(2m)}$ , i.e.  $\ell_t|\nabla n_0|/n_0 \ll 1$  (see Supplemental Material, SM [29]), we find operator-valued Poisson's equation

$$\ell_t^2 \nabla^2 \hat{\phi}_+(\mathbf{r}) \approx \left(1 - \frac{\hat{n}_+(\mathbf{r}, t)}{n_0(\mathbf{r})}\right). \quad (3)$$

The mean density  $n_0(\mathbf{r}) \neq 0$  needs to be measured independently. By measuring  $\hat{n}_+(\mathbf{r}, t)$ , we obtain a scalar

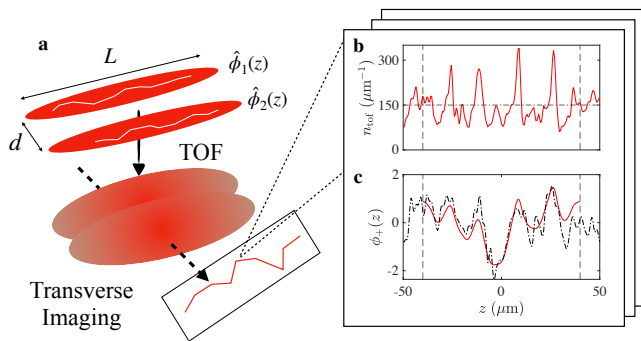


FIG. 1. *Total phase profiles extraction in 1D.*- (a) Parallel 1D Bose gases undergoing free expansion in time of flight (TOF). (b) A simulated example of density ripple  $n_{\text{tof}}(z)$  (solid red) obtained by integrating density after TOF in the radial direction. The dashed-dotted line represents the mean in situ density  $n_0$ . (c) The total phase  $\phi_+^{(\text{out})}(z)$  (solid red) extracted from density ripple in (a). The dashed-dotted line is the numerically imprinted  $\phi_+^{(\text{in})}(z)$ . To avoid edge effects, we only extract  $\phi_+^{(\text{out})}(z)$  between the dashed lines  $z \in [-\mathcal{L}/2, \mathcal{L}/2]$  with  $\mathcal{L} < L$  and  $L$  is the initial length of the gas (before TOF). The full statistics of the field  $\hat{\phi}_+(z)$  is reconstructed by repeating measurements over many shots.

density distribution  $n_+(\mathbf{r}, t)$  which is related to the single-shot total phase profile  $\phi_+(\mathbf{r})$  through Eq. (3). Extracting  $\phi_+(\mathbf{r})$  is then solving the corresponding Poisson's equation, whose solution is unique up to a constant for a given boundary condition. This argument can be extended to the case of unequal mean density, and an arbitrary number of quasicondensates, including a single quasicondensate [29].

*Effects of interference.*- We now apply our method to a quantum field simulator consisting of two parallel 1D quasi-condensates, where interference is measured. Each quasi-condensate is described by a field operator  $\hat{\psi}_{1,2}(z) = e^{i\hat{\phi}_{1,2}(z)} \sqrt{(n_0(z)/2) + \delta\hat{n}_{1,2}(z)}$  which evolves according to low-energy Hamiltonian of the system. Here, we make no assumption about the system's natural evolution and only focus on the measurement process.

In typical experiments, the two gases are imaged after time of flight (TOF), where they are released from the trap and allowed to expand (see Fig. 1a). The full statistics of the relative phase field  $\hat{\phi}_-(z) = \hat{\phi}_1(z) - \hat{\phi}_2(z)$  is then extracted from density interference patterns [30, 31]. Our goal is to also read out the total phase  $\hat{\phi}_+(z) = \hat{\phi}_1(z) + \hat{\phi}_2(z)$  up to a constant from the longitudinal density fluctuations in the measured interference pattern. Being able to measure both  $\phi_{\pm}(z)$  is relevant for probing interaction between difference and total sectors and for full tomography of the system. Similar to  $\hat{\phi}_{\pm}(z)$ , we define the relative and total fields for the density fluctuations  $\delta\hat{n}_{\pm}(z) = \delta\hat{n}_1(z) \pm \delta\hat{n}_2(z)$ .

We will show that our method still works even in the

presence of interference (cross terms in the total densities). To measure  $\phi_+(z)$ , we focus on interfered 1D longitudinal density

$$n_{\text{tof}}(z, t_{\text{tof}}) = \int dr |\Psi_1(r, z, t_{\text{tof}}) + \Psi_2(r, z, t_{\text{tof}})|^2, \quad (4)$$

where  $\Psi_{1,2}$  include both transverse and radial components of the fields,  $r$  denotes radial position and  $t_{\text{tof}}$  is the expansion time. Without loss of generality we assume the in situ ( $t_{\text{tof}} = 0$ ) radial component of  $\Psi_{1,2}$  to be Gaussian of width  $\sigma_0 = \sqrt{\hbar/(m\omega_{\perp})}$  localized around  $(x, y) = (\pm d/2, 0)$  with  $d > \sigma_0$ . Meanwhile, the in situ longitudinal component is modelled as stochastic scalar fields in the truncated Wigner approximation [32, 33], where each scalar field is interpreted as a single experimental realization. The evolved fields  $\Psi_{1,2}(r, z, t_{\text{tof}})$  are related to the in situ fields through TOF dynamics, which we model as ballistic expansion [18, 19, 26], i.e.  $\Psi_{1,2}(r, z, t_{\text{tof}}) = \int d^3\mathbf{r}' G^{(3)}(\mathbf{r} - \mathbf{r}', t_{\text{tof}}) \Psi_{1,2}(r', z', 0)$  with  $G(\xi, t) = \sqrt{m/(2\pi i \hbar t)} \exp[-m\xi^2/(2i\hbar t)]$  being the free particle propagator.

Employing asymptotic expansion technique [19, 34], we show that (see SM [29])

$$n_{\text{tof}}(z) \approx n_0(z) + \delta n_+(z) - \frac{\hbar t_{\text{tof}}}{2m} \partial_z (n_0(z) \partial_z \phi_+(z)), \quad (5)$$

which takes the form of a linearized continuity Eq. (2) with total current  $j_+(z) = (\hbar/2m)n_0(z)\partial_z\phi_+(z)$ . This implies we can extract both  $\phi_-(z)$  and  $\phi_+(z)$  from the same interference picture. Eq. (5) clarifies the relation between density ripple  $n_{\text{tof}}(z)$  and in situ fluctuation of  $\phi_+(z)$ , see Fig. 1b-c. In positions where  $\partial_z j_+ > 0$  ( $\partial_z j_+ < 0$ ), there is more mass going out (in) than going in (out) of an infinitesimal element, leading to depletion (accumulation) of local density during the expansion.

If we next assume that the mean density varies slowly over a length scale  $\ell_{\text{tof}} \equiv \sqrt{\hbar t_{\text{tof}}/(2m)}$ , i.e.  $(\ell_{\text{tof}} \partial_z n_0)/n_0 \ll 1$  and ignore density fluctuation, we will obtain the 1D Poisson's Eq. (3), which we solve by expanding in Fourier modes

$$\phi_+^{(\text{out})}(z) \equiv \sum_{k>0} \text{Re}(A_k) \cos(kz) + \text{Im}(A_k) \sin(kz), \quad (6)$$

and solve for  $A_k$  (setting  $A_0 = 0$ ). Above,  $k = 2\pi p/\mathcal{L}$ ,  $p$  is a positive integer, and  $\mathcal{L}$  is the relevant extraction length. The result is

$$A_k = \frac{-2}{(k\ell_{\text{tof}})^2} \frac{1}{\mathcal{L}} \int_{-\mathcal{L}/2}^{\mathcal{L}/2} \left(1 - \frac{n_{\text{tof}}(z, t_{\text{tof}})}{n_0(z)}\right) e^{ikz} dz. \quad (7)$$

Our extraction method ignores the effect of in situ density fluctuation and terms beyond linear order in  $t_{\text{tof}}$  [29]. The former introduces noise while the latter results in our estimator having finite resolution determined by  $\ell_{\text{tof}}$ , i.e. the modes where  $k\ell_{\text{tof}} > 1$  get quadratically suppressed,

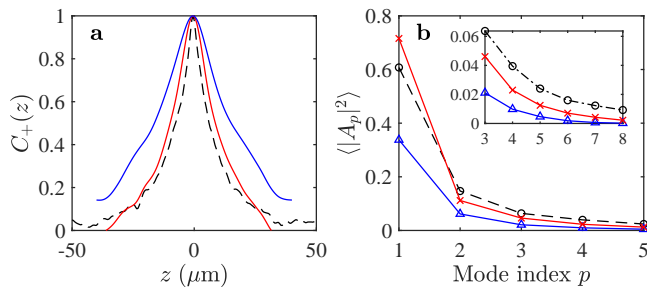


FIG. 2. *Total phase extraction performance.*- (a) Correlation function  $C_+(z)$  for  $T_+ = 50$  nK computed using extracted phases  $\{\phi_+^{\text{(out)}}(z)\}$  with  $t_{\text{tof}} = 11$  ms (red) and  $t_{\text{tof}} = 20$  ms (blue). The dashed black line is  $C_+(z)$  computed with input samples  $\{\phi_+^{\text{(in)}}(z)\}$ . (b) The spectrum  $\langle |A_p|^2 \rangle$  with mode index  $1 \leq p \leq 5$  corresponding to momentum  $|k| = 2\pi p/L$ . The black circle is for the input samples, red cross (blue triangle) is our reconstruction with  $t_{\text{tof}} = 11$  ms ( $t_{\text{tof}} = 20$  ms). The inset is for  $3 \leq p \leq 8$ . The suppression of the extracted  $\langle |A_p|^2 \rangle$  is mostly due to linearization of the TOF dynamics, which worsens the resolution for longer  $t_{\text{tof}}$ . In both panels, statistics are obtained with  $10^3$  shots. Other parameters are  $T_- = 30$  nK,  $n_0 = 150 \mu\text{m}^{-1}$ ,  $L = 100 \mu\text{m}$ ,  $\mathcal{L} = 80 \mu\text{m}$ ,  $d = 3 \mu\text{m}$ ,  $\omega_{\perp} = 2\pi \times 2$  kHz and  $m$  is the mass of  $^{87}\text{Rb}$ .

rendering our extraction effective only for fluctuations with  $k \leq \ell_{\text{tof}}^{-1}$ .

*Extraction performance.*- We evaluate the extraction performance through numerical simulation. The simulation consists of three stages: i) sampling in situ phase and density fluctuations, ii) simulating TOF dynamics which encodes the sampled phases into the density distribution, and iii) reconstructing the encoded total phase from density ripple data.

We sample the in situ fluctuations from Bogoliubov modes [35, 36] assuming decoupled uniform gases and neglecting quantum (zero temperature) fluctuations

$$\phi_+^{\text{(in)}}(z) = \sqrt{\frac{4k_B T_+}{n_0 L}} \sum_{k \neq 0} \sqrt{\frac{|\ln \xi_k|}{E_k}} \sin(kz + 2\pi \xi'_k), \quad (8)$$

where  $T_+$  is the temperature of the total sector,  $E_k = (\hbar k)^2/2m$  is the free dispersion, and  $\xi_k, \xi'_k \in [0, 1]$  are independently sampled uniform random variables. A similar expansion holds for the relative phase and density fluctuations [29]. We then propagate the fields with free particle Green's function, compute the density ripple  $n_{\text{tof}}(z)$ , and readout the total phase  $\phi_+^{\text{(out)}}(z)$  via Eqs. (6)-(7). We repeat the procedure for  $10^3$  shots. A single-shot example is shown in Fig. 1b-c.

To validate our extraction, we study the total phase correlation function [9, 12, 37]

$$C_+(z) = \langle \cos[\phi_+(z) - \phi_+(0)] \rangle, \quad (9)$$

where  $\langle \rangle$  denotes the average over realizations. For a uniform thermal state,  $C_+(z)$  decays exponentially

with a length scale of thermal coherence length  $\lambda_{T_+} = 2\hbar^2 n_0 / (mk_B T_+)$ . By fitting  $C_+(z)$ , we can directly measure the temperature  $T_+$ , thereby providing an alternative method to density ripple thermometry [26, 38].

The reconstruction of  $C_+(z)$  for  $T_+ = 50$  nK is shown in Fig. 2a for two different expansion times,  $t_{\text{tof}} = 11$  ms and  $t_{\text{tof}} = 20$  ms. The former has a better resolution which leads to a better reconstruction of  $C_+(z)$ . This result indicates the correction term to the linearized continuity Eq. (5) plays a more important role for longer  $t_{\text{tof}}$ . In addition, we show in SM [29] that our estimator can faithfully reconstruct the full contrast distribution function [31].

We also study the Fourier spectrum  $\langle |A_p|^2 \rangle$ , which is directly proportional to the modes' mean energy. Except for  $t_{\text{tof}} = 11$  ms and  $p = 1$ , the reconstructed mean energy is upper-bounded by the in situ mean energy (see Fig. 2b). The lost energy is most likely due to our linear approximation, although some could go to other sectors during TOF dynamics [19]. Meanwhile, the added energy in  $p = 1$  and  $t_{\text{tof}} = 11$  ms case is partly due to noise from longitudinal expansion, relative phase, and in situ density fluctuation (see SM [29]).

*Experimental data analysis.*- We next demonstrate total phase extraction by analyzing an ultra-cold atom experiment. At  $t = -t_0$ , two parallel and independent 1D quasicondensates are prepared in a thermal state and trapped in a box-like potential. The latter is realized by superimposing the harmonic magnetic potential with a blue-detuned laser light with the central part of the atomic cloud blocked by a mask. For details see SM [29].

At  $-t_0 < t < 0$ , the second phononic mode  $k_2 = 2\pi/L$  is excited by modulating the amplitude of the dipole light at the resonant frequency  $\omega_2 = ck_2$ ,  $c$  being the speed of sound. The modulation excites the total phase mode resonant to the drive, thereby imprinting a specific single-mode phase pattern to be reconstructed. At  $t \geq 0$ , we stop the driving and let the system evolve. The dynamics of the system is probed by performing density measurements  $n_{\text{tof}}(z)$  after 11.2 ms TOF, at different evolution times and repeated over  $\sim 130$  experimental shots for each evolution time.

Figs. 3a-b show the extraction of the total phase in thermal equilibrium ( $t = -t_0$ ) from experimental data. As expected from a thermal state, we obtain a vanishing first moment  $\langle \delta\phi_+^{\text{(th)}}(z) \rangle = 0$ . An exponential fit to the correlation function  $C_+(z)$  yields the thermal coherence length  $\lambda_{T_+} = 12.8 \pm 0.6 \mu\text{m}$  equivalent to temperature  $T_+ = 56 \pm 3$  nK, which is only slightly lower than  $T_+ = 62 \pm 4$  nK obtained with density ripple thermometry [26, 38].

After the system is let to naturally evolve ( $t > 0$ ), we expect  $\phi_+(z)$  to be the sum of two contributions, i) excitation due to laser modulation  $\phi_+^{\text{(mod)}}(z)$  and ii) thermal fluctuation  $\delta\phi_+^{\text{(th)}}(z)$ . On average, thermal contribution

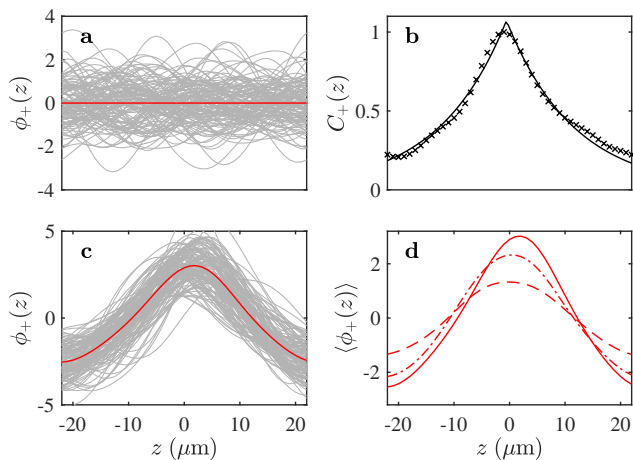


FIG. 3. *Experimental data analysis.*- (a) Extracted  $\phi_+(z)$  in thermal equilibrium. Each grey line represents a single realization of  $\phi_+(z)$  and the red line shows the mean signal  $\langle\phi_+(z)\rangle$ . (b) Thermal phase correlation function (crosses) and the fitted (solid) line  $C_+(z) = a \exp(|z - z_0|/\lambda_{T_+})$  with  $a, z_0, \lambda_{T_+}$  being the fit parameters. From the fit, we extract a temperature of  $T_+ = 56 \pm 3$  nK. (c) Single shots (grey) and mean (red) total phase at  $t = 10$  ms after the driving is turned off. We observe clear excitation of the resonant mode ( $k_2 = 2\pi/L$ ) in the mean signal. (d) Damped recurrence of resonant mode excitation at  $t = 10$  ms (solid),  $t = 40$  ms (dashed-dotted), and  $t = 70$  ms (dashed). Density ripple data is obtained with  $t_{\text{tof}} = 11.2$  ms. The length of the box potential is  $L \approx 46 \pm 3 \mu\text{m}$ , the extraction length is  $\mathcal{L} \approx 46.2 \mu\text{m}$ , and the mean background density  $n_0 \approx 64 \mu\text{m}^{-1}$ . The evolution is probed with a time step  $\Delta t = 5$  ms and  $\sim 130$  shots at each time step.

vanishes so we expect the first moment to contain only the modulation signal  $\langle\phi_+(z)\rangle \approx \langle\phi_+^{(\text{mod})}(z)\rangle$ . In Fig. 3c, we show both the fluctuations and the mean signal at  $t = 10$  ms. As we expect, the mean signal displays a clear excitation of the resonant mode. We observe recurrence of the signal as expected for Luttinger liquids. In Fig. 3d, we show the mean signal recurring with  $\tau_1 \approx 30$  ms period. The observed amplitude damping can be due to corrections to the effective Luttinger liquid model [39] or due to other sources of dissipation.

*Summary & Outlook.*- We have presented a method to measure total phase fluctuations for two parallel quasicondensates. We then applied our method to extract the total phase profiles of two parallel 1D Bose gases from density ripple after matter-wave interference and validated our extraction through numerical simulations and experiments.

The principle behind our extraction is linearization of the continuity equation, which is a general principle that can be applied not just to 1D systems. Indeed, our formulation can be extended into  $N$  quasicondensates of arbitrary dimension. Therefore, the method can be applied in a variety of other systems with spatial phase

gradients such as 2D gases [40, 41], cold atoms in optical lattices [42–45], and superfluid vortices [46]. One can also improve the method by solving the continuity equation without linearization. Our method enables tackling relaxation dynamics [21–23, 36], testing the applicability limits of low-energy effective models [23, 47–49], and performing full quantum field tomography [20, 50]. Thus, our work expands the scope and capabilities of quantum field simulation for studying quantum matter in and out of equilibrium.

*Acknowledgments.*- We thank Mohammadamin Tajik for the useful discussions. TM, MG, and NN were supported through the start-up grant of the Nanyang Assistant Professorship of Nanyang Technological University, Singapore which was awarded to NN. Additionally, MG has been supported by the Presidential Postdoctoral Fellowship of the Nanyang Technological University. The experiments in Vienna are supported by the Austrian Science Fund (FWF) [Grant No. I6276, QuFT-Lab] and the ERC-AdG: *Emergence in Quantum Physics* (EmQ).

\* fiqurtadho@gmail.com

† nelly.ng@ntu.edu.sg

- [1] I. M. Georgescu, S. Ashhab, and F. Nori, *Rev. Mod. Phys.* **86**, 153 (2014).
- [2] E. Altman, K. R. Brown, G. Carleo, L. D. Carr, E. Demler, C. Chin, B. DeMarco, S. E. Economou, M. A. Eriksson, K.-M. C. Fu, M. Greiner, K. R. Hazzard, R. G. Hulet, A. J. Kollár, B. L. Lev, M. D. Lukin, R. Ma, X. Mi, S. Misra, C. Monroe, K. Murch, Z. Nazario, K.-K. Ni, A. C. Potter, P. Roushan, M. Saffman, M. Schleier-Smith, I. Siddiqi, R. Simmonds, M. Singh, I. Spielman, K. Temme, D. S. Weiss, J. Vučković, V. Vuletić, J. Ye, and M. Zwierlein, *PRX Quantum* **2**, 017003 (2021).
- [3] A. J. Daley, *Nature Reviews Physics* **5**, 702 (2023).
- [4] I. Bloch, J. Dalibard, and S. Nascimbene, *Nat. Phys.* **8**, 267 (2012).
- [5] C. Gross and I. Bloch, *Science* **357**, 995 (2017).
- [6] C. Viermann, M. Sparn, N. Liebster, M. Hans, E. Kath, Á. Parra-López, M. Tolosa-Simeón, N. Sánchez-Kuntz, T. Haas, H. Strobel, *et al.*, *Nature* **611**, 260 (2022).
- [7] T. Langen, R. Geiger, and J. Schmiedmayer, in *Annual Review of Condensed Matter Physics*, Vol. 6, edited by J. Langer (2015) pp. 201–217.
- [8] M. Gring, M. Kuhnert, T. Langen, T. Kitagawa, B. Rauer, M. Schreitl, I. Mazets, D. A. Smith, E. Demler, and J. Schmiedmayer, *Science* **337**, 1318 (2012).
- [9] T. Langen, R. Geiger, M. Kuhnert, B. Rauer, and J. Schmiedmayer, *Nat. Phys.* **9**, 640 (2013).
- [10] M. Tajik, M. Gluza, N. Sebe, P. Schüttelkopf, F. Cataldini, J. Sabino, F. Møller, S.-C. Ji, S. Erne, G. Guarnieri, *et al.*, *PNAS* **120**, e2301287120 (2023).
- [11] T. Langen, S. Erne, R. Geiger, B. Rauer, T. Schweigler, M. Kuhnert, W. Rohringer, I. E. Mazets, T. Gasenzer, and J. Schmiedmayer, *Science* **348**, 207 (2015).
- [12] B. Rauer, S. Erne, T. Schweigler, F. Cataldini, M. Tajik,

- and J. Schmiedmayer, *Science* **360**, 307 (2018).
- [13] M. Tajik, I. Kukuljan, S. Sotiriadis, B. Rauer, T. Schweigler, F. Cataldini, J. Sabino, F. Møller, P. Schüttelkopf, S.-C. Ji, *et al.*, *Nat. Phys.*, **1** (2023).
- [14] S. Aimet, M. Tajik, G. Tournaire, P. Schüttelkopf, J. Sabino, S. Sotiriadis, G. Guarnieri, J. Schmiedmayer, and J. Eisert, “Experimentally probing landauer’s principle in the quantum many-body regime,” (2024), arXiv:2407.21690 [quant-ph].
- [15] V. Gritsev, A. Polkovnikov, and E. Demler, *Phys. Rev. B* **75**, 174511 (2007).
- [16] T. Schweigler, V. Kasper, S. Erne, I. Mazets, B. Rauer, F. Cataldini, T. Langen, T. Gasenzer, J. Berges, and J. Schmiedmayer, *Nature* **545**, 323 (2017).
- [17] D. A. Smith, S. Aigner, S. Hofferberth, M. Gring, M. Andersson, S. Wildermuth, P. Krüger, S. Schneider, T. Schumm, and J. Schmiedmayer, *Optics Express* **19**, 8471 (2011).
- [18] Y. D. van Nieuwkerk, J. Schmiedmayer, and F. Essler, *SciPost Phys.* **5**, 046 (2018).
- [19] T. Murtadho, M. Gluza, K. Z. Arifa, S. Erne, J. Schmiedmayer, and N. H. Y. Ng, (2024), arXiv:2403.05528 [cond-mat.quant-gas].
- [20] M. Gluza, T. Schweigler, B. Rauer, C. Krumnow, J. Schmiedmayer, and J. Eisert, *Commun. Phys.* **3**, 12 (2020).
- [21] A. A. Burkov, M. D. Lukin, and E. Demler, *Phys. Rev. Lett.* **98**, 200404 (2007).
- [22] I. Mazets and J. Schmiedmayer, *Eur. Phys. J. B* **68**, 335 (2009).
- [23] S. Huber, M. Buchhold, J. Schmiedmayer, and S. Diehl, *Phys. Rev. A* **97**, 043611 (2018).
- [24] S. Dettmer, D. Hellweg, P. Ryytty, J. J. Arlt, W. Ertmer, K. Sengstock, D. S. Petrov, G. V. Shlyapnikov, H. Kreutzmann, L. Santos, and M. Lewenstein, *Phys. Rev. Lett.* **87**, 160406 (2001).
- [25] D. Hellweg, S. Dettmer, P. Ryytty, J. Arlt, W. Ertmer, K. Sengstock, D. Petrov, G. Shlyapnikov, H. Kreutzmann, L. Santos, *et al.*, *Appl. Phys. B* **73**, 781 (2001).
- [26] A. Imambekov, I. E. Mazets, D. S. Petrov, V. Gritsev, S. Manz, S. Hofferberth, T. Schumm, E. Demler, and J. Schmiedmayer, *Phys. Rev. A* **80**, 033604 (2009).
- [27] S. Manz, R. Bücker, T. Betz, C. Koller, S. Hofferberth, I. E. Mazets, A. Imambekov, E. Demler, A. Perrin, J. Schmiedmayer, and T. Schumm, *Phys. Rev. A* **81**, 031610 (2010).
- [28] P. E. Tavares, A. R. Fritsch, G. D. Telles, M. S. Hussein, F. Impens, R. Kaiser, and V. S. Bagnato, *PNAS* **114**, 12691 (2017).
- [29] See Supplementary Material.
- [30] T. Schumm, S. Hofferberth, L. M. Andersson, S. Wildermuth, S. Groth, I. Bar-Joseph, J. Schmiedmayer, and P. Krüger, *Nat. Phys.* **1**, 57 (2005).
- [31] S. Hofferberth, I. Lesanovsky, T. Schumm, A. Imambekov, V. Gritsev, E. Demler, and J. Schmiedmayer, *Nat. Phys.* **4**, 489 (2008).
- [32] M. J. Steel, M. K. Olsen, L. I. Plimak, P. D. Drummond, S. M. Tan, M. J. Collett, D. F. Walls, and R. Graham, *Phys. Rev. A* **58**, 4824 (1998).
- [33] A. Sinatra, C. Lobo, and Y. Castin, *Journal of Physics B: Atomic, Molecular and Optical Physics* **35**, 3599 (2002).
- [34] C. M. Bender and S. A. Orszag, *Advanced mathematical methods for scientists and engineers I: Asymptotic methods and perturbation theory* (Springer Science & Business Media, 2013).
- [35] H.-P. Stimming, N. J. Mauser, J. Schmiedmayer, and I. E. Mazets, *Phys. Rev. Lett.* **105**, 015301 (2010).
- [36] H.-P. Stimming, N. J. Mauser, J. Schmiedmayer, and I. E. Mazets, *Phys. Rev. A* **83**, 023618 (2011).
- [37] P. Ruggiero, L. Foini, and T. Giamarchi, *Phys. Rev. Res.* **3**, 013048 (2021).
- [38] F. Møller, T. Schweigler, M. Tajik, J. a. Sabino, F. Cataldini, S.-C. Ji, and J. Schmiedmayer, *Phys. Rev. A* **104**, 043305 (2021).
- [39] F. Cataldini, F. Møller, M. Tajik, J. a. Sabino, S.-C. Ji, I. Mazets, T. Schweigler, B. Rauer, and J. Schmiedmayer, *Phys. Rev. X* **12**, 041032 (2022).
- [40] S. Sunami, V. P. Singh, D. Garrick, A. Beregi, A. J. Barker, K. Luksch, E. Bentine, L. Mathey, and C. J. Foot, *Phys. Rev. Lett.* **128**, 250402 (2022).
- [41] S. Sunami, V. P. Singh, D. Garrick, A. Beregi, A. J. Barker, K. Luksch, E. Bentine, L. Mathey, and C. J. Foot, *Science* **382**, 443 (2023).
- [42] A. Impertro, S. Karch, J. F. Wienand, S. Huh, C. Schweizer, I. Bloch, and M. Aidelsburger, (2023), arXiv:2312.13268 [cond-mat.quant-gas].
- [43] Y. Nakamura, Y. Takasu, J. Kobayashi, H. Asaka, Y. Fukushima, K. Inaba, M. Yamashita, and Y. Takahashi, *Phys. Rev. A* **99**, 033609 (2019).
- [44] M. Atala, M. Aidelsburger, M. Lohse, J. T. Barreiro, B. Paredes, and I. Bloch, *Nature Physics* **10**, 588 (2014).
- [45] P. T. Brown, D. Mitra, E. Guardado-Sanchez, R. Nourafkan, A. Reymbaut, C.-D. Hébert, S. Bergeron, A.-M. Tremblay, J. Kokalj, D. A. Huse, *et al.*, *Science* **363**, 379 (2019).
- [46] S. Inouye, S. Gupta, T. Rosenband, A. P. Chikkatur, A. Görlitz, T. L. Gustavson, A. E. Leanhardt, D. E. Pritchard, and W. Ketterle, *Phys. Rev. Lett.* **87**, 080402 (2001).
- [47] Y. D. van Nieuwkerk and F. H. L. Essler, *SciPost Phys.* **9**, 025 (2020).
- [48] J.-F. Mennemann, I. E. Mazets, M. Pigneur, H. P. Stimming, N. J. Mauser, J. Schmiedmayer, and S. Erne, *Phys. Rev. Res.* **3**, 023197 (2021).
- [49] A. Imambekov and L. I. Glazman, *Science* **323**, 228 (2009).
- [50] A. Steffens, M. Friesdorf, T. Langen, B. Rauer, T. Schweigler, R. Hübener, J. Schmiedmayer, C. A. Ríofrío, and J. Eisert, *Nat. Commun.*, 7663.
- [51] T. Schweigler, “Correlations and dynamics of tunnel-coupled one-dimensional bose gases,” (2019), arXiv:1908.00422 [cond-mat.quant-gas].
- [52] D. A. Smith, M. Gring, T. Langen, M. Kuhnert, B. Rauer, R. Geiger, T. Kitagawa, I. Mazets, E. Demler, and J. Schmiedmayer, *New J. Phys.* **15**, 075011 (2013).
- [53] S. Hofferberth, I. Lesanovsky, B. Fischer, J. Verdu, and J. Schmiedmayer, *Nature Physics* **2**, 710 (2006).
- [54] I. Lesanovsky, T. Schumm, S. Hofferberth, L. M. Andersson, P. Krüger, and J. Schmiedmayer, *Physical Review A* **73**, 033619 (2006).
- [55] I. Lesanovsky, S. Hofferberth, J. Schmiedmayer, and P. Schmelcher, *Physical Review A* **74**, 033619 (2006).

### Appendix A: Generalization to $N$ quasicondensates and unequal mean density for $N = 2$

In this section, we provide the detailed derivation of the operator-valued Poisson's equation connecting the total phase  $\hat{\phi}_+(\mathbf{r}) = \sum_a \hat{\phi}_a(\mathbf{r})$  and the total density  $\hat{n}_+(\mathbf{r}, t) = \sum_a \hat{n}_a(\mathbf{r}, t)$  for arbitrary number of quasicondensates  $a = 1, 2, \dots, N$ . We start with a general continuity equation for the total density

$$\partial_t \hat{n}_+(\mathbf{r}, t) + \frac{\hbar}{m} \sum_a \nabla \cdot \left( n_a(\mathbf{r}, t) \nabla \hat{\phi}_a(\mathbf{r}, t) \right) = 0. \quad (\text{S-1})$$

If we linearize this with respect to evolution time  $t$ , we will obtain Eq. (2) in the main text, which we rewrite for clarity

$$\hat{n}_+(\mathbf{r}, t) \approx \hat{n}_+(\mathbf{r}, 0) - \frac{\hbar t}{m} \sum_a \nabla \cdot \left( n_a(\mathbf{r}, 0) \nabla \hat{\phi}_a(\mathbf{r}, 0) \right). \quad (\text{S-2})$$

Next, we assume that all initial mean densities are equal at  $t = 0$ , i.e.  $n_a(\mathbf{r}, 0) = n_0(\mathbf{r})/N$ . From here onwards, the omission of the time argument implies  $t = 0$ . The first term of Eq. (S-2) can be written as a sum of average and fluctuating term  $\hat{n}_+(\mathbf{r}, 0) = n_0(\mathbf{r}) + \delta \hat{n}_+(\mathbf{r})$  with  $\delta \hat{n}_+(\mathbf{r}) = \sum_a \delta \hat{n}_a(\mathbf{r})$  is the total density fluctuation. We then obtain

$$\hat{n}_+(\mathbf{r}, t) \approx n_0(\mathbf{r}) + \delta \hat{n}_+(\mathbf{r}) - \ell_t^2 \nabla \cdot \left( n_0(\mathbf{r}) \nabla \hat{\phi}_+(\mathbf{r}) \right) \quad (\text{S-3})$$

where  $\ell_t \equiv \sqrt{\hbar t / (Nm)}$  is the dynamic length scale also defined in the main text. To get to the Poisson equation, we assume that the mean density varies slowly over a length scale of dynamic length  $\ell_t |\nabla n_0| / n_0 \ll 1$  so that

$$\ell_t^2 \nabla^2 \hat{\phi}_+(\mathbf{r}) \approx \left( 1 - \frac{\hat{n}_+(\mathbf{r}, t)}{n_0(\mathbf{r})} \right) + \frac{\delta \hat{n}_+(\mathbf{r})}{n_0(\mathbf{r})}, \quad (\text{S-4})$$

assuming  $n_0(\mathbf{r}) \neq 0$ . In Eq. (3) in the main text, we further ignore the density fluctuation term.

When the system of quasicondensates does not have identical mean densities, the current operator is no longer a simple function of the total phase fluctuations. However, extraction can still be done for a simple case of  $N = 2$ . In this context, the linearized continuity equation is

$$\hat{n}_+(\mathbf{r}, t) \approx n_0(\mathbf{r}) + \delta \hat{n}_+(\mathbf{r}) - \frac{\hbar t}{m} \nabla \cdot \left( n_1(\mathbf{r}) \nabla \hat{\phi}_1(\mathbf{r}) + n_2(\mathbf{r}) \nabla \hat{\phi}_2(\mathbf{r}) \right), \quad (\text{S-5})$$

where  $n_0(\mathbf{r}) = n_1(\mathbf{r}) + n_2(\mathbf{r})$  still denotes the total initial mean density. We perform a change of variables into relative and total phases  $\hat{\phi}_\pm(\mathbf{r}) = \hat{\phi}_1(\mathbf{r}) \pm \hat{\phi}_2(\mathbf{r})$ , which gives us

$$\hat{n}_+(\mathbf{r}, t) \approx n_0(\mathbf{r}) + \delta \hat{n}_+(\mathbf{r}) - \ell_t^2 \nabla \cdot \left( n_0(\mathbf{r}) \nabla \hat{\phi}_+(\mathbf{r}) \right) - \ell_t^2 \nabla \cdot \left( \Delta n(\mathbf{r}) \nabla \hat{\phi}_-(\mathbf{r}) \right) \quad (\text{S-6})$$

where  $\Delta n(\mathbf{r}) = n_1(\mathbf{r}) - n_2(\mathbf{r})$  is the mean density imbalance,  $\ell_t \equiv \sqrt{\hbar t / (2m)}$  is the dynamic length scale for  $N = 2$ . If, we again assume that the total mean densities and the mean density imbalance vary slowly with respect to  $\ell_t$ , we obtain a correction to the source term for the operator-valued Poisson equation

$$\ell_t^2 \nabla^2 \hat{\phi}_+(\mathbf{r}) \approx \left( 1 - \frac{\hat{n}_+(\mathbf{r}, t)}{n_0(\mathbf{r})} \right) - \frac{\Delta n(\mathbf{r})}{n_0(\mathbf{r})} \ell_t^2 \nabla^2 \hat{\phi}_-(\mathbf{r}) + \frac{\delta \hat{n}_+(\mathbf{r})}{n_0(\mathbf{r})}. \quad (\text{S-7})$$

Thus, information about the Laplacian of the relative phase is important to correctly reconstruct the total phase. This information can be provided by extracting the relative phase from interference pictures.

### Appendix B: Longitudinal dynamics asymptotic expansion

In this section, we will derive the linearized continuity equation in the presence of interference following time of flight [Eq. (5) in the main text]. We assume that the in situ transverse components of the Bosonic fields are separated from their longitudinal components, and they are given by a Gaussian of width  $\sigma_0 = \sqrt{\hbar / (m\omega_\perp)}$ . Note that throughout



the derivation, we will ignore the interaction-induced broadening of  $\sigma_0$  [51] which breaks separability. We then start with a field of the form

$$\Psi_{1,2}(x, y, z, 0) = \frac{1}{\sqrt{\pi\sigma_0^2}} \exp\left[-\frac{(x \pm d/2)^2 + y^2}{2\sigma_0^2}\right] \psi_{1,2}(z), \quad (\text{S-8})$$

where  $\psi_{1,2} = \sqrt{\frac{1}{2}n_0(z) + \delta n_{1,2}(z)} e^{i\phi_{1,2}(z)}$  is the longitudinal component of the fields. Integrating this field with the radial part of the free particle Green's function, we obtain the field after some expansion time  $t$  (assuming  $\omega_\perp t \gg 1$ )

$$\begin{aligned} \Psi_{1,2}(x, y, z, t) \approx & \frac{1}{\sqrt{\pi\sigma_t^2}} \exp\left(-\frac{(x \pm d/2)^2 + y^2}{2\sigma_t^2}\right) \exp\left(\frac{im[(x \pm d/2)^2 + y^2]}{2\hbar t}\right) \times \\ & \int_{-L/2}^{L/2} dz' G(z - z', t) e^{i\phi_{1,2}(z')} \sqrt{\frac{n_0(z')}{2}} \left(1 + \frac{\delta n_{1,2}(z')}{n_0(z')}\right), \end{aligned} \quad (\text{S-9})$$

where  $d$  is the separation between the two 1D quasicondensates and  $\sigma_t = \sigma_0 \sqrt{1 + \omega_\perp^2 t^2}$  is the expanded Gaussian width. Note that we have used Taylor expansion to linearize the effect of density fluctuations assuming  $\delta n_{1,2}(z) \ll n_0(z)$ .

Here, we are concerned with the superposition of the two fields

$$\Psi(x, y, z, t) = \Psi_1(x, y, z, t) + \Psi_2(x, y, z, t). \quad (\text{S-10})$$

Substituting Eq. (S-9) to Eq. (S-10) and adopting another approximation that  $d \ll \sigma_t$ , we can simplify the total field into

$$\begin{aligned} \Psi(x, y, z, t) \approx & A e^{-\frac{x^2 + y^2}{2\sigma_t^2}} \int_{-L/2}^{L/2} dz' G(z - z', t) \sqrt{\frac{n_0(z')}{2}} \left[ \left(1 + \frac{\delta n_1(z')}{n_0(z')}\right) e^{i\phi_1(z')} e^{iqx/2} \right. \\ & \left. + \left(1 + \frac{\delta n_2(z')}{n_0(z')}\right) e^{i\phi_2(z')} e^{-iqx/2} \right], \end{aligned} \quad (\text{S-11})$$

where  $A$  is normalization constant that absorbs the global phase factor and  $q = md/(\hbar t)$  is inverse fringe spacing. To connect to experimentally measurable quantities, we introduce symmetric (+) and anti-symmetric (-) fields

$$\delta n_\pm(z) = \delta n_1(z) \pm \delta n_2(z) \quad \phi_\pm(z) = \phi_1(z) \pm \phi_2(z), \quad (\text{S-12})$$

and write down Eq. (S-11) in terms of these fields. We then obtain

$$\begin{aligned} \Psi(x, y, z, t) \approx & 2A e^{-\frac{x^2 + y^2}{2\sigma_t^2}} \int_{-L/2}^{L/2} dz' G(z - z', t) e^{i\phi_+(z')/2} \left[ \sqrt{\frac{n_0(z') + \delta n_+(z')}{2}} \cos\left(\frac{qx + \phi_-(z')}{2}\right) \right. \\ & \left. + \sqrt{\frac{n_0(z') - \delta n_-(z')}{2}} \frac{\delta n_-(z')}{n_0(z')} i \sin\left(\frac{qx + \phi_-(z')}{2}\right) \right]. \end{aligned} \quad (\text{S-13})$$

From now on, we will ignore the second term in the square bracket since  $\delta n_-/n_0 \ll 1$ . We then write down the norm of Eq. (S-13) integrated with respect to the vertical  $y$ -axis as

$$\rho_{\text{tof}}(x, z, t) \equiv \int_{-\infty}^{\infty} dy |\psi(x, y, z, t)|^2 = 4|A|^2 e^{-x^2/\sigma_t^2} \left| \int_{-L/2}^{L/2} dz' G(z - z', t) I(x, z', t) \right|^2, \quad (\text{S-14})$$

where

$$I(x, z', t) \equiv \sqrt{\frac{n_0(z') + \delta n_+(z')}{2}} e^{i\phi_+(z')/2} \cos\left(\frac{qx + \phi_-(z')}{2}\right). \quad (\text{S-15})$$

is the integrand function. In the simulation, we integrate Eq. (S-14) numerically. Note that  $\delta n_-$  effect is already ignored in the simulation.

Here, we will further simplify the expression by adopting asymptotic expansion technique [19, 34]. We treat longitudinal dynamics perturbatively by performing Taylor expansion of  $I(x, z', t)$  around small  $\Delta z \equiv z' - z$ . In other words, we write

$$I(x, z', t) = I(x, z, t) + \Delta z \partial_z I + \frac{\Delta z^2}{2} \partial_z^2 I + O(\Delta z^3). \quad (\text{S-16})$$

The physical intuition for this expansion is that for a small enough expansion time, only local regions (small  $\Delta z$ ) influence each other. One could also think of it as averaging over a fastly oscillating Green's function kernel at  $z'$  far away from  $z$ .

Let us consider only the zeroth order term, equivalent to freezing longitudinal dynamics

$$\begin{aligned} \rho_{\text{tof}}^{(0)}(x, z, t) &\approx 4|A|^2 e^{-x^2/\sigma_t^2} \left| I(x, z, t) \int_{-L/2}^{L/2} G(\Delta z, t) d(\Delta z) \right|^2 \\ &\approx |A|^2 e^{-x^2/\sigma_t^2} (n_0(z) + \delta n_+(z)) [1 + \cos(qx + \phi_-(z))]. \end{aligned} \quad (\text{S-17})$$

where we have extended the Green's function integral from  $[-L/2, L/2]$  to  $(-\infty, \infty)$  to get the second line, ignoring finite length correction  $\delta\rho_L(x, z, t)$ . This is justified as long as one is mostly concerned with bulk properties. Note that we have obtained the standard fit formula for extracting relative phase  $\phi_-(z)$  from density after time of flight [19].

We proceed by computing higher-order correction terms. The first order term will vanish for  $L \rightarrow \infty$  because it is proportional to  $\int_{-\infty}^{\infty} (\Delta z G(\Delta z, t)) d(\Delta z) = 0$ . Therefore, the next non-zero correction will come from the second-order term

$$\rho_{\text{tof}}^{(2)}(x, z, t) \approx 4|A|^2 e^{-x^2/\sigma_t^2} \left| I(x, z, t) + \frac{\partial_z^2 I(x, z, t)}{2} \int_{-\infty}^{\infty} (\Delta z^2 G(\Delta z, t)) d(\Delta z) \right|^2. \quad (\text{S-18})$$

It is easy to check that  $\int_{-\infty}^{\infty} (\Delta z^2 G(\Delta z, t)) d(\Delta z) = \frac{i\hbar t}{m} = 2i\ell_{\text{tof}}^2$  with  $\ell_{\text{tof}} \equiv \sqrt{\hbar t/(2m)}$  is the length scale of longitudinal expansion. Defining a derivative with respect to scaled coordinate  $\eta \equiv z/\ell_{\text{tof}}$ , we get

$$\begin{aligned} \rho_{\text{tof}}^{(2)}(x, z, t) &\approx 4|A|^2 e^{-x^2/\sigma_t^2} \left| I(x, z, t) + i\partial_\eta^2 I(x, z, t) \right|^2 \\ &= \rho_{\text{tof}}^{(0)}(x, z, t) + 4|A|^2 e^{-x^2/\sigma_t^2} \left[ -2 \text{Im}(I^* \partial_\eta^2 I) + |\partial_\eta^2 I|^2 \right]. \end{aligned} \quad (\text{S-19})$$

To obtain the linearized continuity equation, we further approximate by ignoring the term  $|\partial_\eta^2 I|^2$ . This term is proportional to fourth-order derivatives with respect to  $\eta$ , which is small for sufficiently smooth mean density and phase fluctuations. Then, the equation is simplified into

$$\rho_{\text{tof}}^{(2)}(x, z, t) \approx \rho_{\text{tof}}^{(0)}(x, z, t) - 8|A|^2 e^{-x^2/\sigma_t^2} \text{Im}(I^* \partial_\eta^2 I). \quad (\text{S-20})$$

We now need to compute  $\text{Im}(I^* \partial_\eta^2 I)$ . For simplicity, we will ignore density fluctuation in the calculation of  $\text{Im}(I^* \partial_\eta^2 I)$ , i.e. we set  $\delta n_+ \rightarrow 0$ . By direct calculation, one can easily verify that

$$\text{Im}(I^* \partial_\eta^2 I) \approx -\frac{n_0(z)}{8} (\partial_\eta \phi_+) (\partial_\eta \phi_-) \sin(qx + \phi_-(z)) + \frac{1}{8} \partial_\eta (n_0 \partial_\eta \phi_+) [1 + \cos(qx + \phi_-(z))]. \quad (\text{S-21})$$

Substituting Eq. (S-21) to Eq. (S-20) and combining it with Eq. (S-17) gives

$$\begin{aligned} \rho_{\text{tof}}^{(2)}(x, z, t) &= |A|^2 e^{-x^2/\sigma_t^2} \{n_0(z) + \delta n_+(z) - \partial_\eta (n_0 \partial_\eta \phi_+)\} [1 + \cos(qx + \phi_-(z))] \\ &\quad + |A|^2 e^{-x^2/\sigma_t^2} n_0(z) \partial_\eta \phi_+ \partial_\eta \phi_- \sin(qx + \phi_-(z)). \end{aligned} \quad (\text{S-22})$$

Now, we are finally in a position to compute the density ripple up to the second order in the integral expansion

$$n_{\text{tof}}(z, t) \approx \int_{-\infty}^{\infty} \rho_{\text{tof}}^{(2)}(x, z, t) dx. \quad (\text{S-23})$$

To compute this integral, we use the following fact

$$\int_{-\infty}^{\infty} e^{-x^2/\sigma_t^2} \cos(qx + \phi_-(z)) dx = \sqrt{\pi} \sigma_t e^{-(q\sigma_t/2)^2} \cos \phi_-(z), \quad (\text{S-24})$$



which can be ignored in our case since  $q\sigma_t \approx m\omega_\perp d^2/4\hbar \approx 40$  for typical experimental values so that the integral is of order  $10^{-17}$ . The same argument applies to the sine integral.

Finally, after rewriting the derivatives with respect to  $z$  again, we find

$$n_{\text{tof}}(z, t) = n_0(z) + \delta n_+(z) - \frac{\hbar t}{2m} \partial_z (n_0(z) \partial_z \phi_+) + \text{correction terms}, \quad (\text{S-25})$$

where the correction terms include all factors we exclude, such as those proportional to  $(\delta n_-/n_0)$ ,  $\delta\rho_L$ , and  $|\partial_\eta^2 I|^2$ . We have then reproduced the linearized continuity equation in the presence of interference following TOF [Eq. (5) in the main text].

### Appendix C: Bogoliubov sampling for in situ fluctuations

In this section, we will derive the formula for sampling the in situ fluctuations. We start with a prescription from Bogoliubov sampling [36]

$$\delta n_\pm(z) = \sqrt{\frac{2n_{1\text{D}}}{L}} \sum_{k \neq 0} \sqrt{S_k} B_k^\pm \cos(kz + \zeta_k^\pm) \quad (\text{S-26})$$

$$\phi_\pm(z) = \sqrt{\frac{2}{n_{1\text{D}}L}} \sum_{k \neq 0} \frac{1}{\sqrt{S_k}} B_k^\pm \sin(kz + \zeta_k^\pm) \quad (\text{S-27})$$

where  $n_{1\text{D}} = n_0/2$  is the mean density for a single quasicondensate, and  $S_k$  is the structure factor

$$S_k = \sqrt{\frac{E_k}{E_k + 2gn_{1\text{D}}}}, \quad (\text{S-28})$$

with  $E_k = (\hbar k)^2/2m$  being the free dispersion,  $g = 2\hbar a_s \omega_\perp$  is the 1D interaction strength, and  $a_s = 5.2$  nm is the scattering length. Above,  $k = 2\pi p/L$  and  $p$  are non-zero integers (both positive and negative). In our simulation, we set a hard cut-off for fluctuations with momenta  $|p| > 40$ . Furthermore,  $\zeta_k^\pm$  are uniformly distributed random numbers between 0 and  $2\pi$ . The coefficients  $B_k^\pm$  are random positive numbers whose mean square value carries information about modes' mean energy. If we ignore quantum (zero-temperature), it is given by

$$\langle (B_k^\pm)^2 \rangle = \frac{k_B T_\pm}{\sqrt{E_k(E_k + 2gn_{1\text{D}})}}. \quad (\text{S-29})$$

where  $k_B$  is the Boltzmann constant,  $T_\pm$  are the total and relative sectors' temperatures respectively. By using the Box-Muller transform, we may write

$$B_k^\pm = \sqrt{\langle (B_k^\pm)^2 \rangle} |\ln \xi_k^\pm| \quad \zeta_k^\pm = 2\pi \xi_k^{\prime\pm} \quad (\text{S-30})$$

with  $\xi_k^\pm, \xi_k^{\prime\pm} \in [0, 1]$  are uniform random variables. Putting them all together, we finally find a simplified prescription for sampling in situ fluctuations

$$\delta n_\pm(z) = \sqrt{\frac{k_B T_\pm n_0}{L}} \sum_{k \neq 0} \sqrt{\frac{|\ln \xi_k^\pm|}{E_k + gn_0}} \cos(kz + 2\pi \xi_k^{\prime\pm}) \quad (\text{S-31})$$

$$\phi_\pm(z) = \sqrt{\frac{4k_B T_\pm}{n_0 L}} \sum_{k \neq 0} \sqrt{\frac{|\ln \xi_k^\pm|}{E_k}} \sin(kz + 2\pi \xi_k^{\prime\pm}) \quad (\text{S-32})$$

The last equation corresponding to the + sector is the same as Eq. (8) in the main text.

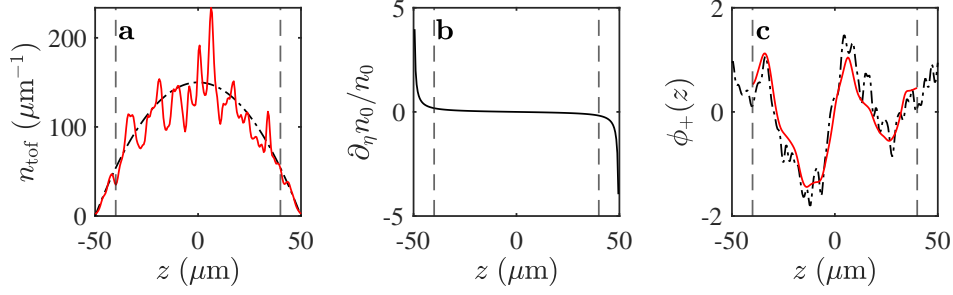


FIG. 4. (a) Density ripple (red) on inverse parabolic mean density profile (dashed black). (b) Scaled derivative of the mean density  $\partial_\eta n_0/n_0$  where  $\eta = z/\ell_{\text{tof}}$ , which is small except near the edges. (c) Reconstructed (red) vs. in situ (dashed black) total phase  $\phi_+(z)$ . The reconstructed profile is obtained by applying our total phase estimator [Eqs. (6)- (7) in the main text] from density ripple shown in panel (a).

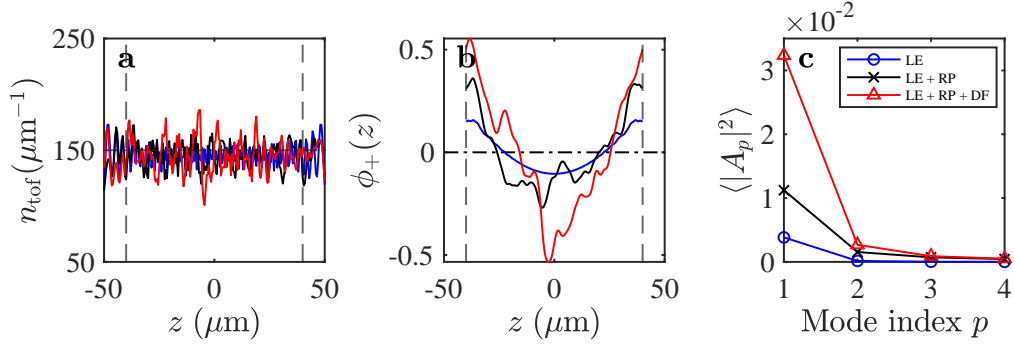


FIG. 5. (a) Contribution of other sectors, i.e. longitudinal expansion (LE), relative phase (RP) and density fluctuation (DF) to the formation of density ripple and error in the extraction of total phase profile. The blue line shows density ripple purely due to LE while the red line shows density ripple due to all combinations of LE + RP + DF. The input total phase is fixed at zero  $\phi_+^{(\text{in})} = 0$ . (b) The readout total phase  $\phi_+^{(\text{out})}$  extracted from the density ripple in (a) is non-zero even though we imprint zero input total phase. The blue color represents the systematic error coming from LE where the edges expand while the bulk remains approximately stationary. The black color is for the case with LE + RP and the red color includes all effects LE + RP + DF (single shot). For a given temperature, the magnitude of the error is small but not negligible when compared to the typical thermal fluctuations of the total phase. (c) The spectrum  $\langle |A_p|^2 \rangle$  of readout total phase fixing zero input signal, taking into account contributions from the different error sources. We see that the systematic coming from density fluctuation is dominant in the fundamental mode ( $p = 1$ ). Expansion time is fixed at  $t_{\text{tof}} = 11$  ms and the statistics are obtained with  $10^3$  shots. Other parameters are the same as in the main text  $T_- = 30$  nK,  $n_0 = 150 \mu\text{m}^{-3}$ ,  $L = 100 \mu\text{m}$ ,  $\mathcal{L} = 80 \mu\text{m}$ ,  $d = 3 \mu\text{m}$ ,  $\omega_\perp = 2\pi \times 2$  kHz,  $a_s = 5.2$  nm, and  $m$  is the mass of  $^{87}\text{Rb}$ .

#### Appendix D: Systematic error analysis, imaging effect, and full contrast distribution function

To solve for  $\phi_+(z)$  given the data of  $n_{\text{tof}}(z, t)$ , we solve the linearized continuity equation, which can be recast into the following dimensionless form

$$\partial_\eta^2 \phi_+ + \left( \frac{\partial_\eta n_0}{n_0} \right) \partial_\eta \phi_+ = 1 - \frac{n_{\text{tof}}}{n_0}. \quad (\text{S-33})$$

In the main text, we ignore the second term on the left-hand side, assuming that  $\partial_\eta n_0/n_0 \ll 1$  in the bulk (excluding edges) valid for sufficiently smooth mean density. In this section, we show that our extraction is robust to correction due to the spatial variation of the mean density. We show an example in Fig. 4 where we accurately extract total phase from density ripple arising from inverse parabolic mean density profile.

However, our analytical derivation and numerical simulation indicate that longitudinal expansion dynamics could induce a systematic error in the extracted total phase, especially near the edges. Analytically, this error comes from the finite length correction  $\Delta\rho_L$ . More physically, this error is due to the motion of the edges of the gas as it is being let go from the trap. This contributes to the overestimation of the fundamental mode's energy [see Fig. 2b in the main text]. We can check this by setting  $\phi_\pm^{(\text{in})}(z) = \delta n_\pm = 0$  and applying our extraction protocol after free expansion.

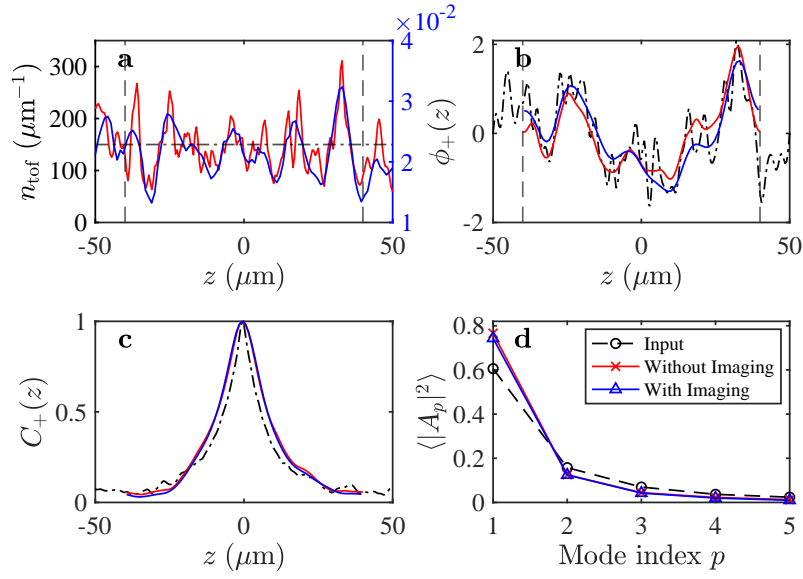


FIG. 6. (a) Density ripple without (red) and with (blue) imaging effect. The scale changes since the imaging system transforms density into intensity in the camera. (b) The comparison between extracted total phase without (red) and with (blue) imaging effect. The dashed-dotted line is the imprinted total phase signal. Total phase correlation function  $C_+(z)$  (c) and spectrum  $\langle |A_p|^2 \rangle$  (d) without (red) and with (blue) imaging effect. We see that our extraction is robust to the effect of imaging both at the level of single shots (b) and at the level of statistics (c-d). Here, expansion time is fixed at  $t_{\text{tof}} = 11$  ms. The pixel size for the transverse imaging system is  $\Delta z \approx 1 \mu\text{m}$  with a resolution of  $\approx 2.5 \mu\text{m}$ . The statistics are obtained with  $10^3$  shots. Other parameters are the same as in the main text  $T_- = 30$  nK,  $n_0 = 150 \mu\text{m}^{-1}$ ,  $L = 100 \mu\text{m}$ ,  $\mathcal{L} = 80 \mu\text{m}$ ,  $d = 3 \mu\text{m}$ ,  $\omega_{\perp} = 2\pi \times 2$  kHz,  $a_s = 5.2$  nm, and  $m$  is the mass of  $^{87}\text{Rb}$ .

In general, the density ripple will not be identical to the mean density (see Fig. 5a) and therefore the extracted phase  $\phi_+^{\text{(out)}}(z)$  will contain a false signal, see Fig. 5b.

We repeat this calibration protocol  $10^3$  times and measure the modes' energy. In the same way, we also check the contribution of symmetric density fluctuation  $\delta n_+$  and relative phase fluctuations  $\phi_-$  to the modes' energies. The result is shown in Fig. 5c. We see that each source of systematic error contributes differently, but they are mostly dominant in the first mode, with density fluctuation being the most dominant.

In the main text, we also ignore the effect of imaging devices. In realistic experiments, the imaging process also induces various effects on density ripple due to many factors such as camera's finite pixel size, defocusing, atoms recoil, and shot noise [51]. These experimental factors effectively introduce an additional momentum cutoff to the density ripple. We simulate the extraction of the total phase without and with imaging systematic effect. The comparison is shown in Fig. 6. We find that our extraction is robust to the effect of imaging, both at the level of single shot and statistics. This adds confidence to the analysis of experimental data contained in the main text.

In addition, here we also consider the reconstruction of the full contrast distribution function  $P(\xi_+)$  [8, 31, 52] with  $\xi_+(l)$  being the integrated contrast defined by

$$\xi_+(l) = \frac{\left| \int_{-l/2}^{l/2} dz e^{i\phi_+(z)} \right|^2}{\left\langle \left| \int_{-l/2}^{l/2} dz e^{i\phi_+(z)} \right|^2 \right\rangle}, \quad (\text{S-34})$$

where  $l$  is allowed to vary between 0 to  $L$ . The corresponding distribution for the relative phase has been used to characterize quantum and thermal noise in Luttinger liquid [31] as well as to study prethermalization after coherent splitting [8, 52]. We find that our total phase estimator faithfully reconstructs the full distribution  $P(\xi_+)$ . We show the comparison between the extracted distribution and the input samples distribution for three different integration lengths  $l = 20 \mu\text{m}, 30 \mu\text{m}, 60 \mu\text{m}$  in Fig. 7.

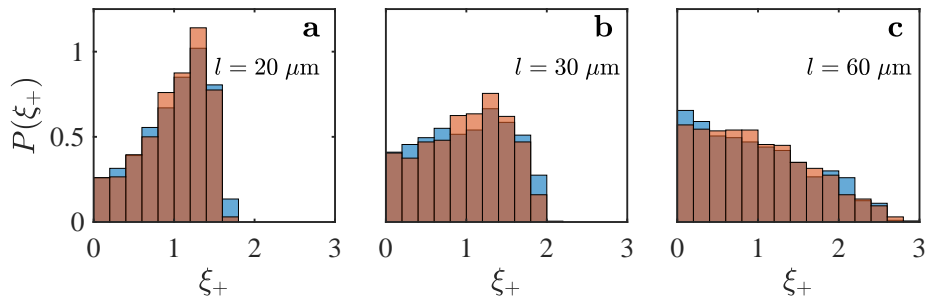


FIG. 7. The full contrast distribution function  $P(\xi_+)$  for  $\xi_+$  defined in Eq. (S-34). The red histogram shows the estimated distribution from our extraction, while the blue histogram shows the distribution computed with the input samples. Each panel correspond to different integration lengths:  $l = 20 \mu\text{m}$  (a),  $l = 30 \mu\text{m}$  (b), and  $l = 60 \mu\text{m}$  (c). We see that our estimator can faithfully reconstruct  $P(\xi_+)$ . Here, the effect of imaging is ignored, but we expect the result to be essentially unchanged. Expansion time is fixed at  $t_{\text{tof}} = 11$  ms. The distribution is obtained with  $10^3$  shots. Other parameters are the same as in the main text  $T_- = 30$  nK,  $n_0 = 150 \mu\text{m}^{-1}$ ,  $L = 100 \mu\text{m}$ ,  $\mathcal{L} = 80 \mu\text{m}$ ,  $d = 3 \mu\text{m}$ ,  $\omega_{\perp} = 2\pi \times 2$  kHz,  $a_s = 5.2$  nm and  $m$  is the mass of  $^{87}\text{Rb}$ .

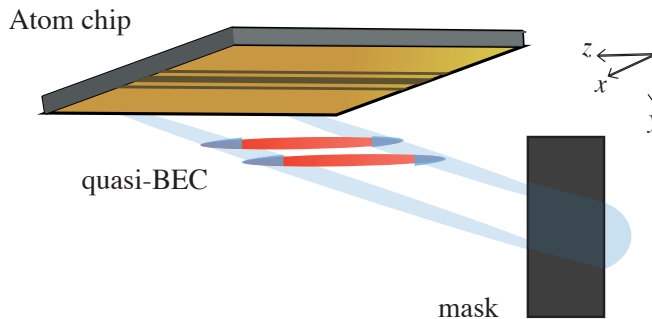


FIG. 8. *Schematics of the box trap setup.* The blue-detuned laser light is sent on a mask which is imaged onto the atoms. The light is blocked from the center of the beam forming a box with steep potential walls. The dipole trap is overlapped with the magnetic harmonic potential generated by the atom chip.

### Appendix E: Experimental setup and protocol

*Experimental setup* - The experiments are performed on our AtomChip [53]. Laser cooled  $^{87}\text{Rb}$  atoms are loaded into a series of magnetic traps and cooled by forced evaporation to bring our system deep into quantum degeneracy and realise a one-dimensional quasi-condensate of  $^{87}\text{Rb}$  atoms. The double well (DW) potential is realized by radio-frequency (RF) dressed-state potentials[53–55]. A box-like trap consists of two parallel and uncoupled cigar-shaped harmonic wells, each with a trap frequency of  $\omega_{\perp} \approx 2\pi \cdot 1.4$  kHz in the two tightly confined directions and  $\omega_z \approx 2\pi \cdot 7$  Hz in the elongated direction.

The box trap along the longitudinal direction is created by shining a blue-detuned laser-light (767 nm) onto a mask from a direction perpendicular to the weakly confined axis of the system. The mask is aligned such that it shields the center of the atomic clouds from the light beam, hence creating two steep walls on the sides. A schematic of the setup is shown in Fig. 8. The dipole potential is overlapped to the harmonic magnetic trap, hence the bottom of the box potential has a small, negligible to our purposes, curvature.

*Experimental protocol* - A thermal state is prepared in the box-shaped uncoupled DW; its temperature is estimated by analyzing the speckle pattern emerging after 11.2 ms of time-of-flight (TOF) [27, 38]. For the experiment presented in the main text, the temperature is 62 (4) nK.

To excite a single density mode the amplitude of the dipole trap is modulated over time at a frequency in resonance with the phononic mode  $\omega_2 = ck_2 = c2\pi/L$ . For the experiment under consideration, the box length is  $L \approx 50 \mu\text{m}$  and speed of sound  $c \approx 1.8 \mu\text{m}/\text{ms}$ , therefore the driving frequency used is  $\omega_2 = 2\pi \cdot 36$  Hz. The modulation lasts for 30 ms, corresponding to approximately one period, after which the system is let equilibrate for 130 ms. The full out-

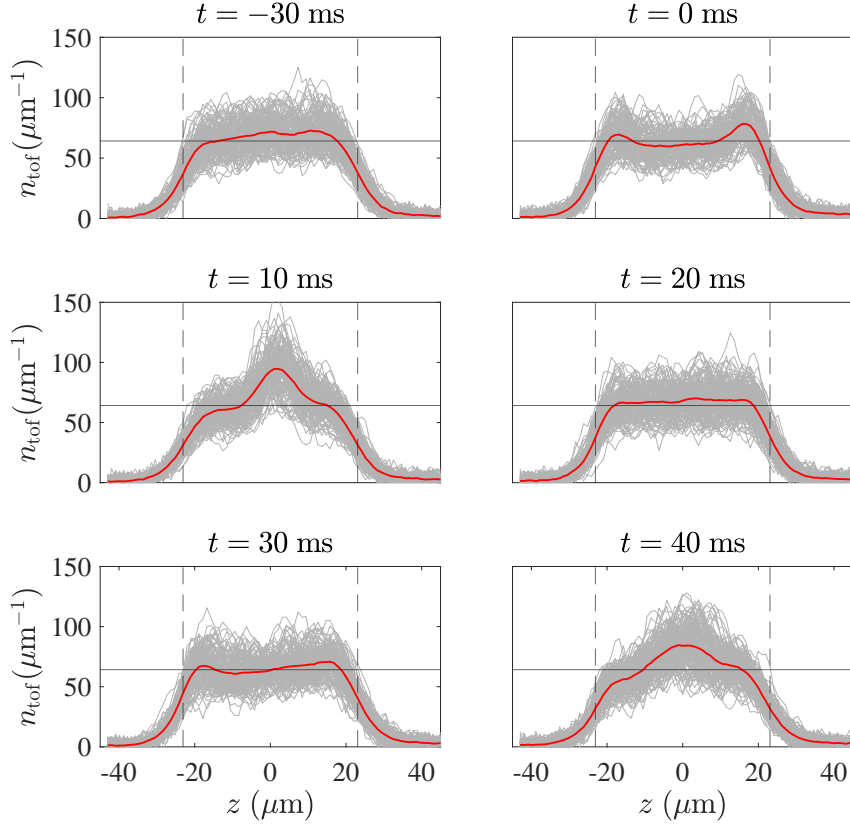


FIG. 9. *Density ripple data from experiment.*- Each panel shows a single realization (grey) and average signal (red) of density ripple  $n_{\text{tof}}(z)$  at different evolution times. The top left panel ( $t = -30$  ms) shows the data in thermal equilibrium (before the driving protocol is on). We then drive the system with frequency resonant to the first mode  $\omega_1 = k_1 c$  with  $k_1 = 2\pi/L$  and  $c$  being the speed of sound. The driving is stopped at  $t = 0$  ms (top right). The system is then let to naturally evolve. The dashed lines indicate the relevant length in which we are extracting the total phase ( $L \approx 46 \pm 3 \mu\text{m}$ ). The black solid line indicates mean linear density  $n_0 \approx 64 \mu\text{m}^{-1}$  calculated in thermal equilibrium ( $t = -30$  ms). In extracting  $\phi_+(z)$ , we also take into account slight spatial variation in mean density  $n_0(z)$  by using the data shown in red line in panel (a). The system's dynamics is probed at every time step  $\Delta t = 5$  ms with 11.2 ms TOF measurement. Experimental repetition for each time step is  $\sim 130$  shots.

of-equilibrium dynamics is monitored by extracting, at each time step, the density profiles  $n_{\text{tof}}(z)$  of the condensates from absorption pictures taken after 11.2 ms of time-of-flight (TOF). We repeat the experimental procedure many times to collect a statistically large set of data. For the experiment under study, we consider approximately 130 repetitions. The ensemble of recorded density profiles and the relative mean profile for selected time steps is shown in Fig. 9.

To obtain the longitudinal density profile of the atomic cloud, the imaging beam is sent from the transverse direction. During the preparation of the experiment, we make sure that the two clouds in the double well are perfectly balanced and uncoupled. Ensuring the symmetry of the system allows us to assume that the two quasicondensates share the same density profiles and the same dynamics.

To better appreciate the evolution of the system during and after the driving, from the recorded density profile  $n_{\text{tof}}(z)$  we extract, at each time step, the density perturbation as  $\Delta n(z, t) = \langle n_{\text{tof}}(z, t) \rangle - \overline{\langle n_{\text{tof}}(z, t) \rangle}$ , where overline denotes the average over time. For long enough evolution times,  $\overline{\langle n_{\text{tof}}(z, t) \rangle}$  is equal to the background density profile. Fig. 10 illustrates the full dynamics of the density perturbation. In the plot, the driving interval is denoted by negative times and  $t = 0$  represents the end of the driving; positive times refer to the evolution subsequent to the driving. During the 130 ms of evolution, heating of the system is negligible and the measured atom loss rate is about 1 atom/ms, with the total atom number being about 3400. The measured loss arises from three-body recombination, collisions with the background gas particles and technical noise.

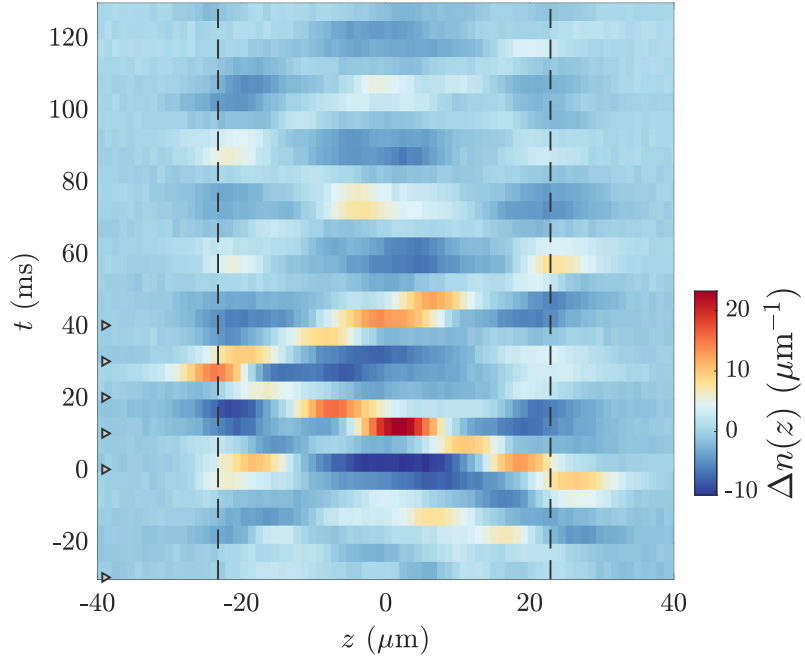


FIG. 10. *Evolution of the mean density perturbation  $\Delta n(z, t)$ .*- Negative times refer to the driving period, while positive times represent the subsequent evolution. The initial time  $-t_0 = -30$  ms corresponds to the initial thermal state. The color map indicates the amplitude of the perturbation over time. The dashed lines mark approximately the position of the box edges, while the small triangles on the side represent some selected time step for which the full density profile  $n_{\text{tot}}(z)$  is shown in Fig. 9.